

Far-infrared Spectral Energy Distribution Fitting for Galaxies Near and Far

Caitlin M. Casey^{1*}

¹ *Institute for Astronomy, University of Hawai'i, 2680 Woodlawn Dr, Honolulu, HI 96822, USA*

Accepted 2012 June 7. Received 2012 May 22; in original form 2012 April 9.

ABSTRACT

Spectral Energy Distribution (SED) fitting in the far-infrared (FIR) is greatly limited by a dearth of data and an excess of free parameters—from galaxies' dust composition, temperature, mass, orientation, opacity, to heating from Active Galactic Nuclei (AGN). This paper presents a simple FIR SED fitting technique joining a modified, single dust temperature greybody, representing the reprocessed starburst emission in the whole galaxy, to a mid-infrared powerlaw, which approximates hot-dust emission from AGN heating or clumpy, hot starbursting regions. This FIR SED can be used to measure infrared luminosities, dust temperatures and dust masses for both local and high- z galaxies with 3 to 10+ FIR photometric measurements. While the fitting technique does not model emission from polycyclic aromatic hydrocarbons (PAHs) in the mid-infrared, the impact of PAH features on integrated FIR properties is negligible when compared to the bulk emission at longer wavelengths.

This fitting method is compared to infrared template SEDs in the literature using photometric data on 65 local luminous and ultraluminous infrared galaxies, (U)LIRGs. Despite relying only on 2–4 free parameters, the coupled greybody/powerlaw SED fitting described here produces better fits to photometric measurements than best-fit literature template SEDs (with residuals a factor of ~ 2 lower). A mean emissivity index of $\beta=1.60\pm 0.38$ and mid-infrared powerlaw slope of $\alpha=2.0\pm 0.5$ is measured; the former agrees with the widely presumed emissivity index of $\beta=1.5$ and the latter is indicative of an optically-thin dust medium with a shallow radial density profile, $\approx r^{-1/2}$. Adopting characteristic dust temperature as the inverse wavelength where the SED peaks, dust temperatures ~ 25 – 45 K are measured for local (U)LIRGs, ~ 5 – 15 K colder than previous estimates using only simple greybodies. This comparative study highlights the impact of SED fitting assumptions on the measurement of physical properties such as infrared luminosity (and thereby infrared-based star formation rate), dust temperature and dust mass, for both local and high-redshift galaxies.

Key words: galaxies: evolution – galaxies: high-redshift – galaxies: infrared – galaxies: starbursts

1 INTRODUCTION

Modeling galaxies' multiwavelength emission has become a sophisticated effort of extragalactic astronomy. Spectral energy distribution (SED) templates, generated by modeling galaxies' stellar populations and radiation, are used prolifically to derive stellar masses, extinction corrections, and stellar ages using broadband photometry from the rest-frame ultraviolet to infrared wavelengths. They are also commonly used to constrain redshifts photometrically (e.g. Bolzonella et al. 2000). The population synthesis-generated

SEDs used to fit short wavelength data ($\lambda \leq 8\mu\text{m}$) are complex (Bruzual & Charlot 2003; Maraston 2005). They depend on the initial mass function (IMF; Salpeter 1955; Kroupa 2001; Chabrier 2003), metallicity, stellar age, and starbursting timescale – duration, frequency, and strength. Although this gives rise to many free parameters in the models, the slew of broadband filters in the optical and near-infrared make this detailed SED fitting possible, even with the effects of dust obscuration/attenuation taken into account (e.g. Calzetti et al. 1994; Calzetti 2001). Follow-up spectral observations in the optical and near-IR often confirm good fits to broadband photometry and accurate stellar population modeling.

* Hubble Fellow; cmcasey@ifa.hawaii.edu

The dawn of new infrared observing facilities—from the *Herschel Space Observatory*, the Atacama Large Millimeter Array (ALMA), to the SCUBA2 instrument on the James Clerk Maxwell Telescope (JCMT)—has triggered a wave of interest in extending the use of these template SED libraries to the far-infrared (FIR; $\sim 8\text{--}1000\mu\text{m}$ rest-frame), for example, in generating far-infrared photometric redshift estimates (Roseboom et al. 2012). Unfortunately, modeling the dust emission from galaxies is just as complex in the far-infrared as it is in the optical since free parameters include dust composition, dust grain type, galaxy structure, orientation, active galactic nuclei (AGN) heating, emissivity, and optical depth. However, in contrast to the optical and near-infrared, far-infrared observations are plagued with a dearth of data. Where there might be 10-20 broadbands in the optical/near-IR, there are at most ~ 8 bands in the FIR (most galaxies having data in 3 bands or less), all of which suffer from the increased beamsize of single-dish FIR observations, thus increasing uncertainty on measured flux.

Nevertheless, detailed radiative transfer models and empirical template libraries have been devised in recent years to model the dust infrared emission of stars, molecular clouds and starburst galaxies over a wide range of bolometric luminosities (Silva et al. 1998; Chary & Elbaz 2001; Dale et al. 2001; Dale & Helou 2002; Abel & Wandelt 2002; Siebenmorgen & Krügel 2007; Draine & Li 2007). These models are then often used as a basis on which to measure the fundamental parameters of observed starburst galaxies with constrained photometric measurements, both at low redshift (e.g. Rieke et al. 2009; Armus et al. 2009; Chapin et al. 2009; U et al. 2012) and at high redshift (e.g. Blain et al. 2002; Chapman et al. 2004; Pope et al. 2008; Swinbank et al. 2010). Particularly for galaxies with high star formation rates, the ‘UV chimney’ argument (Neufeld 1991) can be used to relate the modeled dust and molecular cloud structure back to the Ly- α escape fraction; Ly- α suffers from less attenuation than UV continuum photons despite very large reservoirs of dust and gas.

This paper investigates the use of these far-infrared template SEDs to determine fundamental galaxy properties such as infrared luminosity, L_{IR} , characteristic dust temperature, T_{dust} , and dust mass, M_{dust} . Section 2 presents a simple method for representing galaxies’ FIR emission as a coupled modified greybody plus a mid-infrared (MIR) powerlaw, which can constrain these fundamental IR-derived properties quite well for a wide range of galaxies. Section 3 compares these fits to the SED template fits of Chary & Elbaz (2001), Dale & Helou (2002) and Siebenmorgen & Krügel (2007), using the photometry of local luminous infrared galaxies and ultraluminous infrared galaxies (LIRGs/ULIRGs) from U et al. (2012). Section 4 discusses derived quantities of FIR SED fits, and section 5 concludes. Throughout, a Λ CDM cosmology with $H_0=71\text{ km s}^{-1}\text{ Mpc}^{-1}$ and $\Omega_{\text{m}}=0.27$ is assumed (Hinshaw et al. 2009).

2 SED FITTING TECHNIQUES

2.1 Coupled Greybody/Powerlaw Fitting

2.1.1 Method

Deriving the fundamental physical properties of IR-luminous galaxies can be as simple as assuming an isotropically emitting blackbody. This is represented as the Planck function, $B_{\nu}(T)$ (e.g. in units of $\text{erg s}^{-1}\text{ cm}^{-2}\text{ \AA}^{-1}$), and is only dependent on dust temperature T . However, if the variation in opacity (e.g. assuming a screen of dust without scattering) and source emissivity is accounted for (the fact that very few sources are perfectly non-reflective), the flux density at rest-frame frequency ν is then represented by a modified black body (i.e. ‘greybody’) of the form

$$S(\nu) \propto (1 - e^{-\tau(\nu)})B_{\nu}(T) = \frac{(1 - e^{-\tau(\nu)})\nu^3}{e^{h\nu/kT} - 1} \quad (1)$$

where $S(\nu)$ is in units of $\text{erg s}^{-1}\text{ cm}^{-2}\text{ Hz}^{-1}$ or Jy. Optical depth is $\tau(\nu)$ and fitted as $\tau(\nu) = (\nu/\nu_0)^{\beta}$, where ν_0 is the frequency where optical depth equals unity (Draine 2006) and β represents emissivity, or the spectral emissivity index. See Kovács et al. (2010) for a thorough discussion of the impact on β . The value of β is largely assumed to be 1.5 (and usually ranges 1–2, Hildebrand 1983), although this could be a result of the original wavelengths for which data were gathered on local starbursting samples (Dunne & Eales 2001). Some recent work points to a wider range of β values between 1-2.5 (e.g. Chapin et al. 2011; Casey et al. 2011). The theoretically expected value of ν_0 is 3 THz (i.e. $\lambda_0=100\mu\text{m}$), although this value is unconstrained by data (see discussion in Conley et al. 2011). In the optically thin case, the term $(1 - e^{-\tau(\nu)})$ reduces to ν^{β} , and the flux density simplifies to

$$S_{\text{ot}}(\nu) \propto \nu^{\beta} B_{\nu}(T) = \frac{\nu^{\beta+3}}{e^{h\nu/kT} - 1}. \quad (2)$$

The normal range of dust temperatures expected for a galaxy’s interstellar medium (ISM) heated only by star formation ranges $\sim 20\text{--}60\text{ K}$. When fitted to a greybody (as in Equations 1 or 2), most galaxies have a notable flux density excess at wavelengths shortward of $\approx 50\mu\text{m}$ (see Figure 1, panels A and B). This mid-infrared excess is due to a combination of hotter-dust subcomponents (where dust is more compact) or dust heated by an AGN, and an optically thin medium by which the higher frequency radiation can escape. The disconnect between observed mid-infrared luminosities and predicted Wein-tail luminosities has been studied for quite some time; a quite thorough discussion of dust clouds’ opacity, radial density distributions, and dust mass coefficients (κ_{ν}), impact on observed SED is given in Scoville & Kwan (1976); note in particular the difference between optically thin and optically thick models in the near- and mid-infrared regime.

Non-thermal emission from polycyclic aromatic hydrocarbons (PAH) in starburst galaxies or silicate absorption at $9.7\mu\text{m}$ can contribute to the SED shape in this regime as well; however, their net effect on integrated IR luminosity, differing from a simple mid-infrared powerlaw, is $<10\%$ in most cases (See § 2.2).

While the hot-dust component might be made up of several subcomponents of different warm temperatures, the cold dust modified greybody still dominates the bulk of

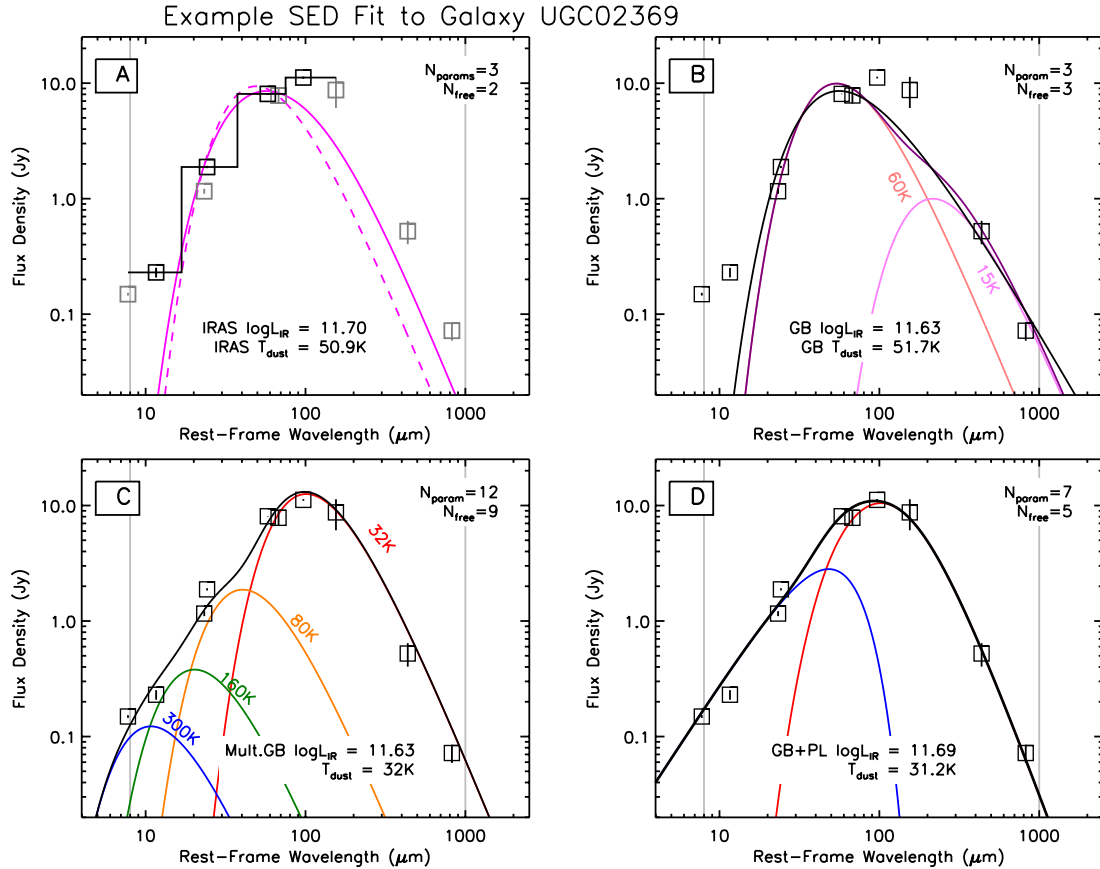


Figure 1. Illustration of FIR SED fitting techniques using the example local galaxy UGC02369. Panel (A) highlights the four *IRAS*-band photometric points in black (the more recent FIR photometric measurements in gray). The original computed FIR luminosity for this source was computed via Eq 5. The original dust temperature for the source (Perault 1987) was found by fitting a single temperature greybody with fixed $\beta=1.5$ to the *IRAS* bands (magenta; the same best-fit SED assuming optically thin conditions is shown in dashed magenta). Panel (B) shows a slightly improved SED fit, with a single temperature greybody fit to all of the FIR photometric bands. Emissivity, β , is added as a free parameter (black) and measured as $\beta=0.5$, which is similar to adding a very cold greybody component to the warm component dominating the emission, both with fixed $\beta \equiv 1.5$ (e.g. 60 K and 15 K SED shown). Both the fits in panels (A) and (B) have mid-infrared excesses and are poor fits to a single temperature greybody. Panel (C) shows an improved fit, using four temperature greybodies with fixed $\beta=1.5$. The fit to the data is much better than (A) or (B), although the number of free parameters shoots up to 9. Panel (D) illustrates the SED fitting technique described in § 2.1, a composite mid-infrared powerlaw plus cold-dust single temperature greybody. The mid-infrared powerlaw is a good approximation for the composite of warm dust giving rise to the mid-IR excess. All fits here assume general opacity conditions; in the optically thin case, the fits alter slightly, but produce the same L_{IR} and T_{dust} to within $\sim 1\%$.

the total infrared emission when integrated. The net sum is an SED which can be approximated as a powerlaw in the mid-infrared, with intensity dropping with decreasing wavelength, and a single temperature greybody fit in the far-infrared. The greybody dominates at wavelengths $>50\mu\text{m}$ whereas the mid-infrared powerlaw dominates at wavelengths $<50\mu\text{m}$. This can be analytically approximated as:

$$S(\lambda) = N_{\text{bb}} \frac{(1 - e^{-\frac{\lambda_0}{\lambda}})^{\beta} (\frac{c}{\lambda})^3}{e^{hc/\lambda kT} - 1} + N_{\text{pl}} \lambda^{\alpha} e^{-\frac{\lambda}{\lambda_c}} \quad (3)$$

where $S(\lambda)$ is in units of Jy, T is the galaxy’s characteristic “cold” dust temperature (in other words, the dust temperature dominating most of the infrared luminosity and dust mass), λ_0 is the wavelength at which optical depth is unity (taken here to be fixed at $\lambda_0=200\mu\text{m}$ as in Conley et al.

2011), β represents the emissivity, α represents the slope of the mid-infrared powerlaw component, and λ_c is the wavelength where the mid-infrared powerlaw turns over and no longer dominates the emission. This simplifies to

$$S_{\text{ot}}(\lambda) = N_{\text{bb,ot}} \frac{(\frac{c}{\lambda})^{\beta+3}}{e^{hc/\lambda kT} - 1} + N_{\text{pl}} \lambda^{\alpha} e^{-\frac{\lambda}{\lambda_c}} \quad (4)$$

in the optically thin case. Note that several works have recognized the utility of adding a mid-infrared powerlaw components to simple greybody fits (e.g. Younger et al. 2009) but tend to fit the two components separately: first the greybody followed by the mid-infrared powerlaw. Coupling the two together and fitting simultaneously makes it possible for a more accurate fit to be made to systems with fewer FIR photometric datapoints.

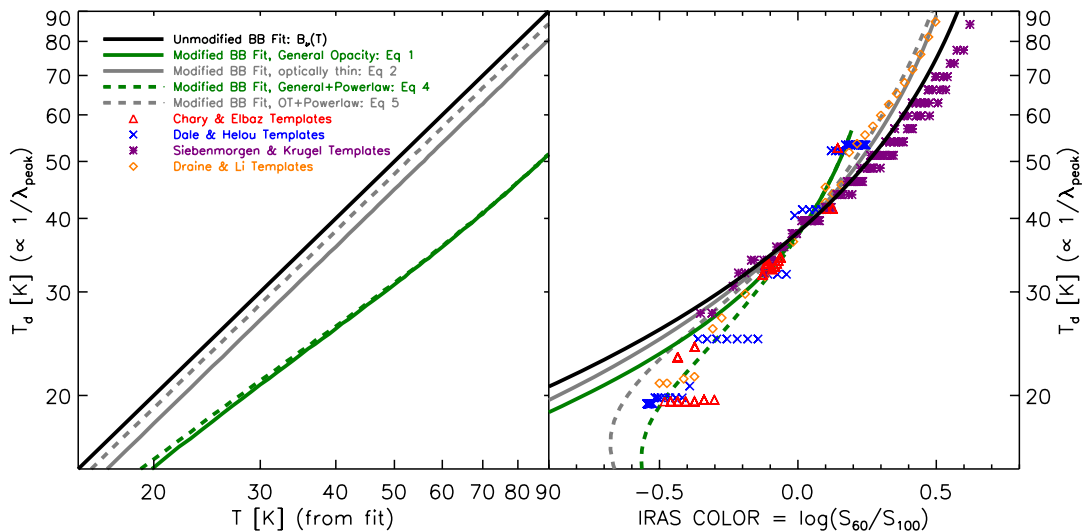


Figure 2. At left, a comparison of the T temperature parameter of the fitted greybody against the “peak wavelength” T_d , which is proportional to the inverse peak in S_ν . This varies by fitting method mostly due to slight variations in adopted opacity, which shifts the SED peak slightly while keeping L_{IR} roughly constant. At right, a comparison T_d , the “peak wavelength” temperature, to *IRAS* [60]-[100] color, which has often been used as a proxy for dust temperature. Over-plotted are various model template values, from Chary & Elbaz (2001), Dale & Helou (2002), Siebenmorgen & Krügel (2007) and Draine & Li (2007).

Figure 1 illustrates this SED fitting technique relative to single temperature greybody fits (as in Eq 1) for an example local LIRG, UGC 02369. This highlights the inconsistency of single temperature greybodies with FIR photometry of real galaxies and the usefulness of an SED fitting technique which simultaneously fits the cold-dust, long-wavelength greybody and mid-infrared excess powerlaw component.

Another common way to consider the ‘warm dust’ components is as a continuous powerlaw distribution of temperature components, e.g. $dM_d/dT \propto T^{-\gamma}$, as described in Kovács et al. (2010). The index γ effectively represents α ; the values $\gamma=7.2$ and $\gamma=6.7$ (both assumed in the Kovács et al. 2010, analysis for different samples) correspond to α values of ≈ 2.9 and 2.6 respectively. Kovács et al. (2010) points out that $\gamma \approx 6.5-7.5$ is expected for sources in a diffuse, star forming medium, and $\gamma \approx 4-5$ for a dense medium from the heating source (e.g. a dusty torus around an AGN). The flux density function is then given as $S_{\nu(T_c \rightarrow \infty)}(T) = (\gamma-1)T^{\gamma-1} \int_T^\infty S_{\nu,T}(T)T^{-\gamma}dT$. This integral must be solved numerically, but leads to an SED of shape similar to those produced by Equations 3 and 4, particularly Equation 3. The differences between the temperature powerlaw integral fit and the analytic approximation in Eq 3 is that the latter provides a bit more flexibility in that the relationship between normalization factors can be adjusted. The former has a clear, robust motivation, but is also a computationally expensive algorithm. As photometry for infrared sources improve and spectroscopy becomes more widely available, a minority of galaxies will likely have unusual SED shapes not well described by $dM_d/dT \propto T^{-\gamma}$, in which case a more general form of Eq 3 might be appropriate.

Note that another popular infrared SED fitting method joins a greybody to a mid-infrared powerlaw using a piecewise technique (Blain et al. 2002, 2003), where the transition point between greybody and powerlaw is defined by $d/d\lambda(S)=\alpha$, i.e. the gradients are equal. This is the most

straightforward way of generating SEDs of the desired shape (panel D of Figure 1). In many instances, this method might be preferred over this paper’s fitting techniques (e.g. when generating hypothetical SEDs for testing selection, or generating fits for galaxies with only one FIR photometric point). However, one disadvantage of this method is its piecewise nature, making it difficult to fit data across the whole infrared range simultaneously and quantify the errors on each parameter. Having an analytic approximation for this functional form (e.g. Equations 3 and 4) makes error propagation and multiple-datapoint fitting much more straightforward.

2.1.2 Adjusting the 2–4 free parameters

There are six total parameters in this fit: the greybody normalization (N_{bb}), the powerlaw normalization (N_{pl}), greybody temperature (T), emissivity index (β), mid-infrared powerlaw slope (α), and mid-infrared turn-over wavelength (λ_c). Since the turnover wavelength of the mid-infrared powerlaw would depend on the turnover point of the cold dust greybody component and N_{pl} determines the flux scaling of the powerlaw term relative to the greybody, neither parameter should not be considered ‘free’ in the sense of the other four. Both λ_c and N_{pl} are tied to the best-fit values of N_{bb} , T and α such that the total SED resembles both the Kovács et al. (2010) powerlaw temperature distribution SED and the Blain et al. (2003) piecewise matched-gradient SED.

The turnover wavelength, λ_c is set to 3/4 the wavelength where the gradient of the greybody is α , as in Blain et al.. λ_c is both a function of α , T and the adopted opacity model, and can be approximated as $\lambda_c = (T \times (a_1 + a_2\alpha))^{-1}$ (optically thin) and $\lambda_c = ((b_1 + b_2\alpha)^{-2} + (b_3 + b_4\alpha) \times T)^{-1}$ (general opacity). The values of the coefficients are given in Table 1. Note that the factor of 3/4 is incorporated so that the juncture of the powerlaw and greybody is

most smooth (i.e. it does not have a physical interpretation, although is related to the falloff rate of e^{-x^2}). The coefficient of the powerlaw term, N_{pl} , is tied to the normalization of the greybody term and solves the condition $N_{\text{pl}}\lambda_c^\alpha = S_\nu(\lambda_c)$, where S_ν is given by Equations 1 or 2. Having fixed these two parameters reduces the number of free parameters to 2–4.

Depending on the amount of FIR photometric data available, further constraints can be made to reduce the number of free parameters in the fit described in Equation 3 or Equation 4 from four (N_{bb} , T , β , and α) to two (N_{bb} and T). The number of free parameters should never exceed the number of independent data points minus one. The emissivity β varies from 1–2.5 in the literature for individual sources, although the vast majority of works assume a fixed value of $\beta=1.5$ (Chapman et al. 2005; Pope et al. 2006; Casey et al. 2009, among others). Varying β does not have a very significant impact on FIR luminosity or dust temperature, but does have a strong impact on the slope of the Rayleigh-Jeans tail at rest-frame $\lambda \geq 200\mu\text{m}$. If there are >3 independent photometric points at $\lambda \geq 200\mu\text{m}$, then β can be constrained with the fit; otherwise, the fixed value of $\beta=1.5$ is suggested. The mid-infrared powerlaw slope can be constrained similarly; if >3 photometric points are available at rest-frame $\lambda \leq 70\mu\text{m}$, then α can be measured. Otherwise, a fixed value of $\alpha=2.0$ is consistent with most sources and is directly comparable to the mid-infrared portion of SED templates presented in the next section. Typical values of α range from 0.5 (nearly flat, consistent with quite a bit of warm dust) to 5.5 (very steep, consistent with very little warm dust). Note that values of $\alpha < 1$ lead to a divergent luminosity in the near-infrared, so some additional cutoff should be placed at short wavelengths to avoid a nonphysical interpretation.

2.1.3 Defining L_{IR} and T_{dust}

The normalization of the fits is governed by the infrared luminosity, L_{IR} , whose integration limits have varied throughout the literature. L_{IR} is intended to represent the bulk of a galaxy’s dust emission. For galaxies which are very infrared-bright ($L_{\text{IR}} > 10^{11} L_\odot$), L_{IR} is a proxy for bolometric luminosity. L_{IR} is most often taken from 8–1000 μm (e.g. Kennicutt 1998). L_{IR} also goes by different names in the literature: L_{TIR} (“total IR”) or L_{FIR} (“far IR”) and can be integrated from 3–1100 μm (e.g. Chapman et al. 2003), 40–120 μm (e.g. Younger et al. 2009), or 40–1000 μm (e.g. Conley et al. 2011). The rest of the paper uses the standard 8–1000 μm integration limits for the sake of consistency with most of the literature; however, if only the cold-dust, star-formation dominated infrared luminosity is desired, more appropriate limits would be 40–1000 μm .

In the initial years of characterizing *IRAS*-detected IR-luminous galaxies, the integrated IR flux was approximated by:

$$F_{\text{FIR}(40-500)} = 1.26 \times 10^{-14} \{2.58 f_{60} + f_{100}\} \quad (5)$$

in W m^{-2} (and where flux densities, f , are given in Jy , see the review in Sanders & Mirabel 1996). Including all *IRAS* bands and integrating over a wider wavelength range, 8–1000 μm , this becomes:

$$F_{\text{IR}(8-1000)} = 1.8 \times 10^{-14} \{13.48 f_{12} + 5.16 f_{25} + 2.58 f_{60} + f_{100}\}. \quad (6)$$

Luminosities are then $L_{\text{IR}} = 4\pi D_L^2 F_{\text{IR}}$. Section 3 discusses the accuracy of this widely accepted luminosity approximation to the U et al. sample.

Note also that the dust temperature T as given in Equations 1–4 represents the intrinsic galaxy temperature, which is different than the inverse “peak wavelength” temperature as measured by Wein’s displacement law, i.e. $\lambda_{\text{max}} = b/T_d$ (where $b = 2.898 \times 10^3 \mu\text{m K}$), which only applies to perfect blackbodies. Figure 2 shows the intrinsic dust temperature T against peak wavelength dust temperature, T_d for the above formulations. Figure 2 also shows T_d against *IRAS* color, $\log(S_{60}/S_{100})$, for Equations 1–4 and the IR template SEDs discussed in the next section.

Far-infrared color is often taken as a proxy for dust temperature. Works in the literature vary the use of different fitting methods, some using IR template fits, some using optically thin greybodies, some including a warm dust component and some not. The convention of referring to a single dust temperature is meaningless unless it refers to the same measurement made with consistent methodology. However, the Wein’s displacement law value of dust temperature, T_d , does not vary greatly between fitting techniques, so it is insensitive to biases in fitting methods, making it a good diagnostic of the characteristic dust temperature for the whole system. Throughout the rest of the paper, T_d is used to represent galaxies’ dust temperatures and this method also permits fair comparisons across literature sources.

2.2 IR Template SEDs

Template spectral energy distributions are taken from four sources, all of which are widely used in the literature to derive values such as L_{FIR} (thus star formation rate, SFR), T_{dust} , and M_{dust} for nearby and high- z galaxies. The first 105 template SEDs are from Chary & Elbaz (2001), whose models are developed to represent existing data from ~ 0.4 –850 μm on nearby galaxies (and which vary as a function of L_{FIR} , T_{dust} and PAH strength). We also use the 64 phenomenological models of Dale et al. (2001), supplemented by FIR/submillimeter data in Dale & Helou (2002). The SEDs from Chary & Elbaz (2001) and Dale & Helou (2002) are the models most frequently used in the literature (e.g. Chapman et al. 2005; Chapin et al. 2009, and many others). However, the radiative transfer model SEDs from Siebenmorgen & Krügel (2007) are also included, and their parameter space spans much more diverse SED types (by varying nuclear radius, visual extinction, ratio of OB stellar luminosity to total, and dust density). While the Siebenmorgen & Krügel (2007) work contains ~ 7000 SEDs, we limit ourselves to the 120 most luminous SEDs, consistent with ULIRG infrared luminosities. Finally, we include 25 of the most IR-luminous models from the PAH-motivated work of Draine & Li (2007) which have been used for high- z samples (e.g. see Marsden et al. 2011).

The primary observable difference between the infrared template SEDs in this section and the coupled greybody/powerlaw is the inclusion of the PAH emission features and silicate absorption features. Readers interested in the relation between PAH emission and FIR dust emission should clearly use template SEDs instead of simple grey-

$$S(\lambda) = N_{\text{bb}} \frac{(1 - e^{-\frac{\lambda_0}{\lambda}})^{\beta} (\frac{\lambda}{\lambda_0})^3}{e^{hc/\lambda kT} - 1} + N_{\text{pl}} \lambda^{\alpha} e^{-\frac{\lambda}{\lambda_c}}^2$$

Free Parameters:	$N_{\text{bb}}, T, (\beta, \alpha)$	
Emissivity	β	1.60 ± 0.38
Mid-IR Powerlaw Slope	α	2.0 ± 0.5
Wavelength where opacity is unity	λ_0	$\equiv 200 \mu\text{m}$
Powerlaw turnover wavelength	λ_c	$\equiv 3/4 L(\alpha, T)$
where $L(\alpha, T) = ((b_1 + b_2 \alpha)^{-2} + (b_3 + b_4 \alpha) \times T)^{-1}$	b_1	26.68
	b_2	6.246
	b_3	1.905×10^{-4}
	b_4	7.243×10^{-5}
Normalization of powerlaw term	N_{pl}	
	$\equiv N_{\text{bb}} \frac{(1 - e^{-(\lambda_0/\lambda_c)^{\beta}}) \lambda_c^{-3}}{e^{hc/\lambda_c kT} - 1}$	
Characteristic Dust Temperature ($\neq T$)	T_{d}	$1/\lambda_{\text{peak}}$

Table 1. Adopted Best-Fit SED fitting equation and measured parameters based on the GOALS sample. The measurement of β is based on 48 out of the 65 galaxies which have 850–1.1 mm data, while the measurement of α is based on the full sample of 65 (U)LIRGs.

body/powerlaw fits. However, in terms of the basic physical properties extracted from FIR SEDs— L_{IR} , T_{dust} , and M_{dust} , there is not a significant detriment to using the greybody/powerlaw fitting technique. The PAH emission lines at 7.7 μm , 11.2 μm , and 12.8 μm contribute to the integrated IR luminosity on the order of 5%, although their contribution is often negated by the presence of the 9.7 μm absorption feature.

The mid-infrared spectra of dusty starbursts have been shown to vary substantially at both low- z and high- z (Brandl et al. 2006; Pope et al. 2008; Menéndez-Delmestre et al. 2009). Without a direct mid-infrared spectrum, it is impossible to know whether or not PAHs or absorption features are contributing significantly to broadband photometric measurements. At certain rest-frame wavelengths, FIR photometric measurements are likely to deviate positively or negatively from a mid-infrared powerlaw (e.g. at $\sim 8 \mu\text{m}$ in the former case and $10 \mu\text{m}$ in the latter case). In those cases, infrared template SEDs should be used to more accurately determine the structure of mid-infrared emission.

3 SED COMPARISONS WITH DATA

Testing and comparing the different IR Template SEDs from Section 2.2 and SED fitting methods from Section 2.1 requires a sample of well-constrained FIR-bright galaxies with accurate FIR photometric measurements. To date, the most extensively imaged IR galaxies—besides the handful of high- z brightly lensed sources (e.g. the “cosmic eyelash,” Swinbank et al. 2010)—are from the local *IRAS*-selected Revised Bright Galaxy Sample (RBGS; Sanders et al. 2003), particularly the subset which form part of the Great-Origins All Sky LIRG Survey (GOALS; Armus et al. 2009). The revised standard-aperture photometry for 65 galaxies in the GOALS sample is summarized and presented in U et al. (2012), and used herein at rest-frame wavelengths 5–2000 μm .

Modified greybodies plus mid-infrared powerlaw SEDs

are fitted to data as described in Section 2.1, specifically to Equation 3, taking both flux density uncertainties and non-detection upper limits into account¹. The general-opacity fits are chosen for this local sample over the optically-thin fits due to a subtle difference in SED shape around rest-frame wavelengths $\sim 20\text{--}40 \mu\text{m}$.

For sources with more than three long-wavelength data points, β is kept as a free parameter; otherwise it is fixed to $\beta=1.5$. Mid-infrared powerlaw slope α is allowed to vary since the number of short-wavelength points ($< 70 \mu\text{m}$) is always more than three. The range of α values is found to vary between $\alpha=0.5\text{--}5.5$. Dust temperature and luminosity are left to vary. Template IR SEDs from Section 2.2 are fitted to data with a χ^2 minimization method, where the normalization (i.e. $N_{\text{bb}} \propto L_{\text{IR}}$) is a free parameter.

Figure 3 shows several randomly-selected examples of best-fit SEDs for GOALS sources. The various best-fit IR templates are colored, while the fitted SED is shown in black. The underlying greybody function to the fitted SED is shown as a dotted line. Since > 8 FIR photometric points exist for the GOALS sample, a dummy SED can also be constructed by linearly extrapolating between photometric points (shown in gray). While this is a rough approximation, the advantage of this extrapolation is that this dummy SED makes no intrinsic assumptions as to SED shape. The subset of sources shown in Figure 3 represents a wide variety of templates and fitted SEDs and is representative of the fits to the whole U et al. (2012) sample.

The residuals of the fits with respect to data are shown in Figure 4. The residual is computed as the difference in $\log S_{\nu}$ between the data points and the best fit SED at each of the following wavelengths: 12 μm , 25 μm , 60 μm , 100 μm , and 850 μm . Figure 4 shows the distribution in the residuals at each wavelength for the U et al. GOALS sample for each fit. Black represents the residuals from the fitting method described in Section 2.1, and the residuals of the IR templates are colored as in Figure 3. At each wavelength, the mean and standard deviation of the residual distribution is given in the top left.

At *all* wavelengths, the fitted SED from Equation 3 is statistically a better fit to the data than any IR templates, despite having fewer free parameters than the SED templates; a summary of derived quantities from this fit is given in Table 1. However, some templates are more accurate than others; the Siebenmorgen & Krügel templates provide the best fit of the templates, significantly better than both Chary & Elbaz and Dale & Helou templates. However, all seem to suffer at short wavelengths where there is naturally no flexibility built into the models. This demonstrates that galaxies’ mid-infrared properties are not tightly correlated with their far-infrared properties, as perhaps previously thought (since 24 μm is often used to infer L_{IR} , e.g. Le Floc’h et al. 2005, on *Spitzer* samples, among many others).

Another reason the Siebenmorgen & Krügel templates have lower residuals than the other two template libraries is that they contain more templates with which to compare the data. Even at the highest luminosity end ($L_{\text{IR}} > 10^{11} L_{\odot}$),

¹ An IDL function `cmcircsed.pro`, which can be used to fit an SED of the form in Eq 3 or Eq 4 to real data, is publicly available at www.ifa.hawaii.edu/~cmcasey/research.html.

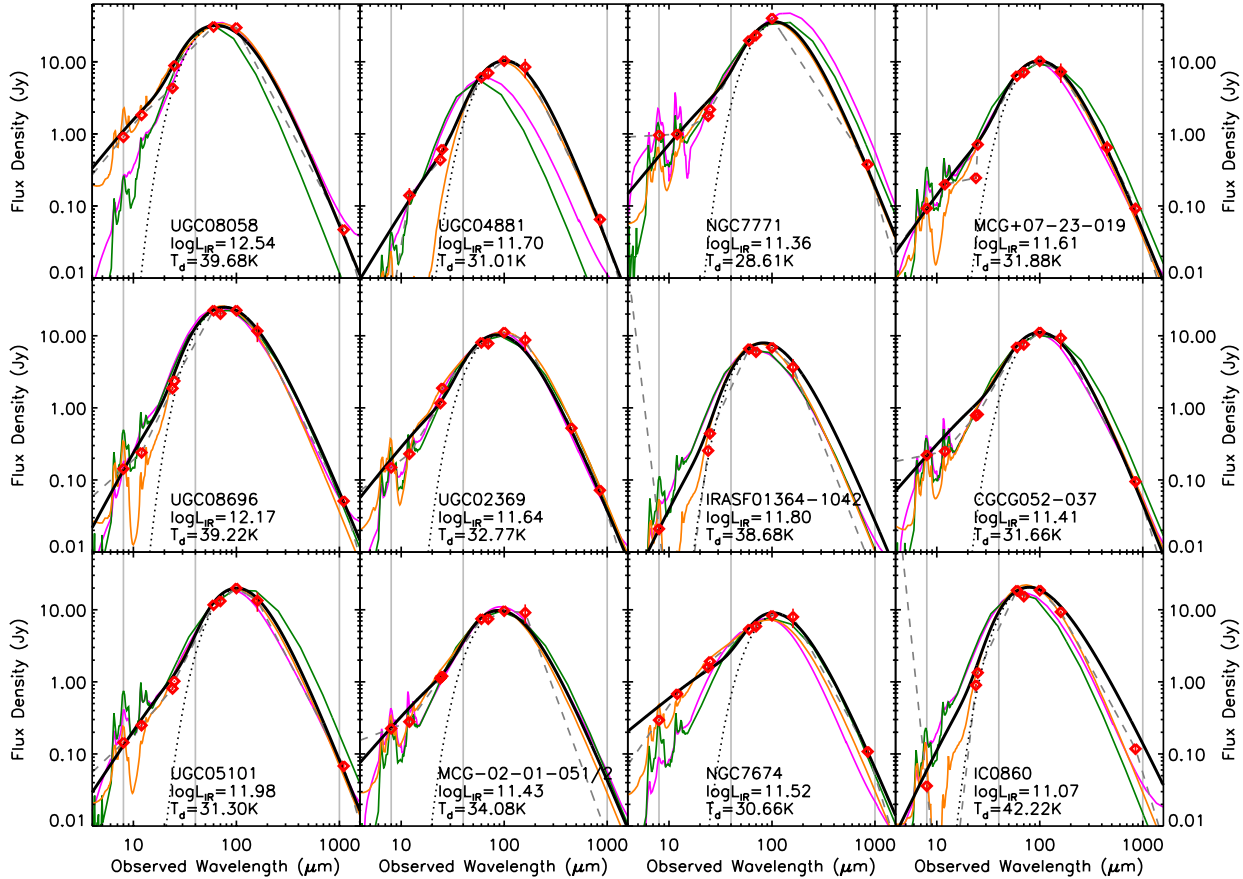


Figure 3. Example best-fit SEDs to a subset of the GOALS sample, whose photometry is presented in U et al. (2012). Photometric data points are shown as red diamonds with uncertainties illustrated (sometimes smaller than the size of the data point). The best-fit SED fit from Equation 3 is shown in black, with the underlying greybody distribution shown as a dotted black line. The best-fit Chary & Elbaz template SED is shown in magenta, Dale & Helou SED shown in green, and Siebenmorgen & Krügel SED shown in orange. A “dummy SED” is also constructed which linearly interpolates between data points in $\log\lambda$ - $\log S_\nu$ space (dashed gray line). The 8–1000 μm and 40–1000 μm integration limits are marked as light gray vertical lines for reference.

there are still 120 template models in the Siebenmorgen & Krügel (2007) library. In contrast, the Chary & Elbaz library contains 105 template SEDs and Dale & Helou contains 64 template SEDs.

This direct comparison between SED fitting and SED templates demonstrates that using IR templates will always provide a less accurate fit than simple greybody/powerlaw fitting. This is not meant to suggest that IR template SEDs are not of great use; on the contrary, they provide very good constraints on the relationships between FIR emission and PAH emission, and sources’ dust composition, which simple greybody fitting cannot do. However, if the purpose of FIR SED fitting is to measure a source’s FIR luminosity, dust temperature and dust mass accurately, this work demonstrates that direct fitting, as in Section 2.1, is best.

3.1 Interpretation of best-fit parameters

The U et al. (2012) sample has been used to constrain the mean SED parameters β , the spectral emissivity index, and α , the mid-infrared powerlaw slope. How do we interpret the measurements $\beta=1.60\pm0.38$ and $\alpha=2.0\pm0.5$? Here I draw on the detailed discussions in Scoville & Kwan (1976).

The measured value of the emissivity index, β , is spot on its presumed value of ≈ 1.5 . Although not new information, this suggests that even the cold dust component (dominating at $\lambda > 50\mu\text{m}$) has a temperature gradient whereby the dust farthest from the luminous starburst is slightly colder, which differentially boosts the flux density at the longest wavelengths. This boosting (above a simple blackbody) becomes enhanced when the density distribution falls off slowly, and with a steep density drop off, β should increase, and the far-infrared “slope” should increase.

The mid-infrared powerlaw slope, α , probes the warmer, more-compact dust, and can be used to estimate the radial density profile. Our measurement of $\alpha=2.0\pm0.5$ agrees with earlier findings of $\alpha=1.7$ – 2.2 from analysis of IRAS and distant galaxies in Blain et al. (2002). Assuming there are sufficient hot dust grains near the interior and the dust is optically thin, $S_\lambda \propto \lambda^\alpha$ where $\alpha=2.0\pm0.5$ translates to a density profile of $r^{-0.5\pm0.2}$, consistent with $r^{-1/2}$. In other words the dust density profile is relatively flat and perhaps indicative of the diffuse nature of the dust around these starbursts, their distributions perhaps originating from the violent interacting nature within the galaxies.

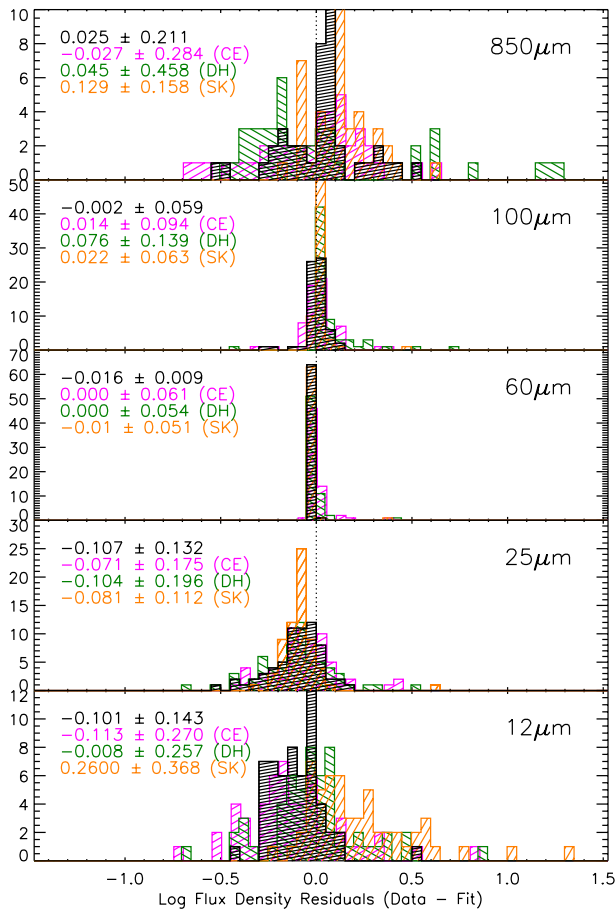


Figure 4. The residuals of the fits to the GOALS sample between template libraries and the coupled greybody/powerlaw fits for all 65 galaxies, for the greybody/powerlaw fits (black), Chary & Elbaz fits (magenta), Dale & Helou fits (green) and Siebenmorgen & Krügel fits (orange). The mean and standard deviations of the residual distributions for each fitting method are given in the upper left-hand corner. The residuals are lowest for greybody/powerlaw fits, followed by the Siebenmorgen & Krügel fits.

4 DERIVED QUANTITIES

Section 3 used the GOALS sample (Armus et al. 2009; U et al. 2012) to demonstrate that direct greybody/powerlaw SED fitting, as described in Section 2.1, is a more accurate fit to data than best-fit IR SED template libraries from the literature. In this section, the derived quantities L_{IR} (luminosity), T_d (dust temperature) and M_d (dust mass) are compared to see what can be expected using different SED fitting methods.

4.1 IR Luminosity and Star Formation Rates

The IR luminosity is most often integrated in the range 8–1000 μm , i.e. $L_{\text{IR}} = 4\pi D_L^2 \int_{\lambda=8\mu\text{m}}^{1000} S_\nu d\nu$. The range 8–1000 μm encompasses some of the most prominent PAH emission features in addition to the greybody emission peak. The boundaries are still somewhat arbitrarily drawn, since 8 μm sits awkwardly on top of the 7.7 μm PAH emission fea-

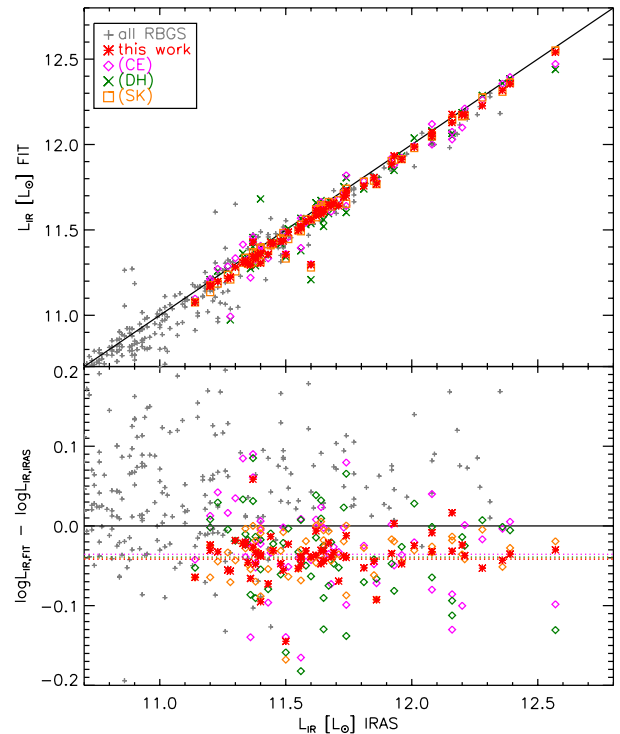


Figure 5. The fitted RBGS IR luminosities, “IRAS luminosities,” are measured as a linear combination of IRAS 12–100 μm flux densities, see Eq 6 or Sanders & Mirabel (1996). Here IRAS luminosities are plotted against fitted luminosities from the direct fitting method (Section 2.1), and template SED libraries. The full RBGS sample of 625 sources from Sanders et al. (2003) is included, and luminosities refitted using IRAS photometry alone and Eq 3, fixing $\beta=1.5$ (scatter is larger for this sample due to poorer photometric constraints). At bottom are the residuals, luminosity against the difference in $\log L_{\text{IR}}$. All template libraries and fitted SEDs demonstrate that IRAS luminosities are overestimated by ~ 0.04 dex, or $\sim 10\%$.

ture, and 1000 μm splits the cold-dust greybody neither at its turnover point, where radio synchrotron emission begins to dominate, nor near the peak. On average, the cold-dust greybody component—thought to be exclusively heated by star-formation processes—comprises $74 \pm 11\%$ of $L_{\text{IR}(8-1000)}$, while warm AGN-heated dust and PAH emission components comprise $26 \pm 11\%$.

Figure 5 shows the 8–1000 μm IR luminosities of the U et al. sample and luminosity residuals when contrasting methods. The x-axis is the IR luminosity as inferred by Equation 6, also as summarized in Sanders & Mirabel (1996) and Armus et al. (2009). The whole RBGS sample is also included, refitting all luminosities using the method from Section 2.1 (due to limited long-wavelength photometry, $\beta=1.5$ is fixed). Similarly, RBGS luminosities are compared to template SED-inferred luminosities. Both the fitted SEDs and template SEDs have lower IR luminosities than predicted using the RBGS Equation (Eq 6) by ~ 0.02 – 0.04 dex. Both Chary & Elbaz and Dale & Helou templates are 0.02 ± 0.07 dex lower in luminosity than IRAS predictions, while Siebenmorgen & Krügel templates are 0.03 ± 0.05 dex

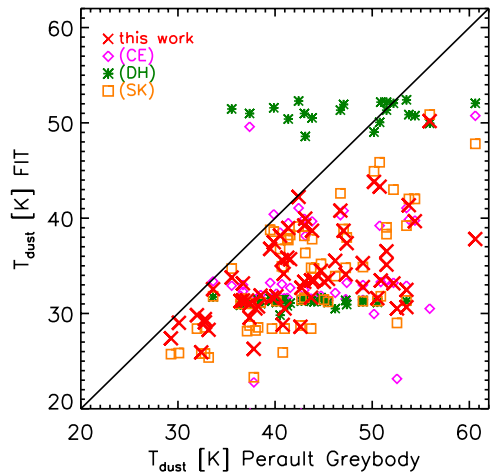


Figure 6. A comparison of dust temperatures from Perault (1987), described also in Sanders & Mirabel (1996), against dust temperatures found using methods in Section 2.1 and from template SEDs. Colors and symbols are as in Figure 5. In all cases, a single greybody fit of the form described in Eq 1 or 2 (which was the method used in Perault 1987) overestimates dust temperature by 10 K on average. Caution is necessary when using dust temperatures from template SEDs since they are quantized.

lower, and fitted SEDs are 0.04 ± 0.04 dex lower. These differences translate to luminosity overpredictions from RBGS of 10%, thus overestimated SFRs by 10%.

Note that the Kennicutt (1998) scaling relation between $L_{\text{IR}(8-1000)}$ and SFR take both the contribution of “infrared circus” cold-dust emission and “warm” dust around young star forming regions into account and is generated using stellar synthesis models (Leitherer & Heckman 1995) for continuous bursts aged 10–100 Myr. Since the Kennicutt scaling is not determined as an empirical relation between, e.g. $H\alpha$ SFR and L_{IR} , there is no need to recalibrate it to correct for the overestimated L_{IR} ; however, the FIR star formation rates of the local (U)LIRG sample should be revised to reflect the systematic offset.

Regardless of the systematic offset, infrared-based star formation rates are only accurate to $\sim 10\%$ mostly due to the variation in mid-infrared properties, likely not directly scaling to the galaxies’ star formation rates, since complex processes dominate the mid-infrared. Similarly, slight changes in any SED which impacts the mid-infrared (e.g. changes in opacity assumptions, assumed α , PAH contributions) will impact the derived star formation rate. For this reason it is worth emphasizing that the systematic offset is of minor significance. Also worth pointing out is that the range 8–1000 μm is not ideal to generate precise star formation rates.

Ideally, one would extract the integrated luminosity from the cold-dust greybody component over all wavelengths where it dominates. This can be estimated precisely if the fitting method in Section 2.1 is used, as the greybody component can then be constructed independently after fitting to a joint greybody and powerlaw. However, to make fair comparisons with different SED fitting methods, the optimal alternative limits of integration should be taken as 40–1000 μm

as in Conley et al. (2011). Longward of 40 μm , the cold-dust greybody dominates at all dust temperatures < 100 K.

4.2 Dust Temperature

Comparing dust temperatures between models first requires an understanding of the dust temperature convention for the original work on the U et al. (2012) GOALS sample objects. Dust temperatures were originally fitted in Perault (1987; PhD Thesis) by fitting a single temperature dust emissivity model ($\epsilon \propto \nu^{-1}$) to the flux in all four *IRAS* bands (briefly described in Sanders & Mirabel 1996). In other words, these dust temperatures are fitted to data ranging 12–100 μm to either Eq 1 or Eq 2. Assumptions made with regard to opacity are not stated; however, the impact on peak dust temperature is minimal. It could be that the dust temperature reported in Perault (1987) is indeed T taken from e.g. Eq 2 rather than “peak wavelength” dust temperature T_d , although it is unclear. Regardless, refitting greybodies of either form specified in Eq 1 or 2 to only the four *IRAS* datapoints causes the dust temperatures T_d to drop by ~ 10 K. This is shown in Figure 6 (and was illustrated clearly in Figure 1, panels A and B). The difference between dust temperatures of simple greybodies and greybodies which incorporate a mid-infrared component has been known (see also the recent detailed discussion in Hayward et al. 2012), yet few works are explicitly clear on how their dust temperature measurements should be interpreted.

The Perault/RBGS dust temperatures are also found to be significantly hotter than dust temperatures measured from the SED template libraries. However, any dust temperatures extracted from the template SEDs should be used with great caution, as the dust temperatures are quantized in all cases (as was seen at right in Figure 2). The Dale & Helou (2002) templates exhibit the poorest constraints on dust temperature, as the templates only have two dust temperatures: $T_d \approx 31$ K and $T_d \approx 51$ K. The Chary & Elbaz (2001) templates have four different dust temperatures, at ≈ 23 K, 32 K, 41 K and 50 K. The Siebenmorgen & Krügel (2007) templates are quantized on yet finer scales, at 5 K increments between ~ 24 K and 85 K; however, the fitted SEDs, as an analytic fit, are not quantized in T_d . For this reason, any dust temperature-based results should be based on fits of the type described in Section 2.1, not on template SEDs in the literature.

4.3 Dust Mass

Dust mass is related to IR flux density and dust temperature via

$$S_\nu = \kappa_\nu B_\nu(T) M_d D_L^{-2} \quad (7)$$

where S_ν is the flux density at frequency ν , κ_ν is the dust mass absorption coefficient at ν , $B_\nu(T)$ is the Planck function at temperature T , M_d is the total dust mass, and D_L is the luminosity distance. The fact that our sources are not perfect black bodies is accounted for by the dust mass coefficient κ_ν so that the greybody is effectively represented by the product $\kappa_\nu B_\nu(T)$, and the sources’ luminosity at frequency ν scales as $S_\nu/B_\nu(T) \propto \nu^{-2}$. The dust mass is then

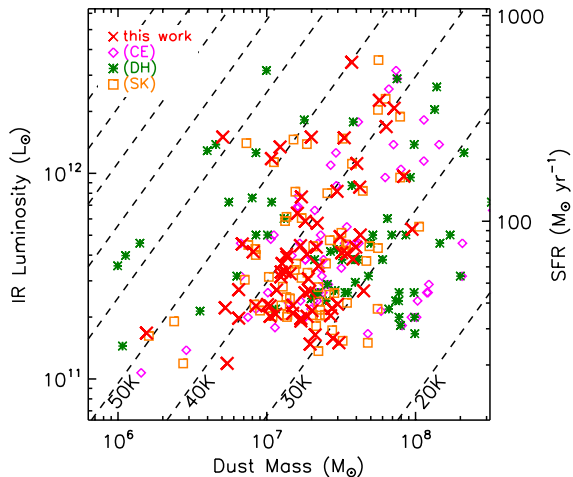


Figure 7. Dust mass against 8-1000 μ m IR luminosity and star formation rate (SFR) measured from the infrared. Isotherms are marked with dashed lines increasing by 10 K. This emphasizes that (a) dust mass is incredibly sensitive to dust temperature and that dust mass should only be computed when dust temperature is adequately constrained, and (b) the lack of correlation between integrated IR luminosity and the Rayleigh-Jeans cold-dust component of IR SEDs (the best probe of dust mass). The latter point points out that using direct scaling relations between, e.g. S_{850} and SFR is not recommended.

$$M_d = \frac{S_\nu D_L^2}{\kappa_\nu B_\nu(T)} \propto \frac{D_L^2}{\kappa_\nu \nu^2}. \quad (8)$$

As Draine et al. (2007) point out, care should be taken when computing dust masses using measured dust temperatures since the thermal emission per unit dust mass at λ is $\propto (e^{hc/\lambda kT} - 1)^{-1}$. At wavelengths $\lambda \leq 360\mu\text{m}$, dust temperature has a profound effect on dust mass, since $B_\nu(T)$ is very dependent on T (so that a 4 K difference between 18 and 22 K results in a 150% increase in M_d). At $\lambda \geq 450\mu\text{m}$, M_d is less sensitive to dust temperature. Note that the dust temperature used in Eq 8 is the T from Eq 3 and not the “peak wavelength” dust temperature T_d characterizing the system as a whole.

Due to poor constraints on dust absorption coefficients and no data points longward of $\sim 450\mu\text{m}$, dust masses for the GOALS sample were not reported until the work of U et al. (2012), who use the method described in this paper, Eq 8, to calculate dust masses at $850\mu\text{m}$ using a dust absorption coefficient of $\kappa_{850} = 0.15 \text{ m}^2 \text{ kg}^{-1}$ (Weingartner & Draine 2001; Dunne et al. 2003). Figure 7 plots the galaxies’ dust masses against IR luminosity, which highlights two important facts. First, the calculation of dust mass is very sensitive to dust temperature, $M_d \propto L_{\text{IR}} T^{-5}$. This highlights that dust mass should *only* be estimated when dust temperature is adequately constrained. The second noticeable detail of Figure 7 is the lack of correlation between the two physical properties, L_{IR} and M_d . The lack of correlation is a testament to how large amounts of dust can be formed quite quickly in starburst galaxies (in contrast, star-forming galaxies with much more moderate star formation rates overall have dust masses several orders of magnitude smaller, $< 10^{5-6} M_\odot$). This also points out that scaling relations where star formation rate is inferred directly from a

long wavelength flux density measurement, e.g. S_{850} , without good constraints on L_{IR} or T , are highly uncertain.

4.4 Future Improvements

The next decade will see great improvements in our understanding of dust emission in galaxies thanks to vast repositories of data from large field-of-view mapping bolometers and efficient follow-up with interferometric imaging. Facilities less limited by confusion noise (e.g. SCUBA-2 $450\mu\text{m}$ mapping on JCMT, and future 200-850 μm data from the Cornell-Caltech Atacama Telescope, CCAT) will make infrared photometric measurements more accurate, precise and more numerous. Submillimeter spectrometers (e.g. like Z-SPEC operated at the Caltech Submillimeter Observatory and Atacama Pathfinder EXperiment, e.g. see Bradford et al. 2009, also those being designed for CCAT) will measure *spectra* for individual sources in the infrared and submillimeter, providing crucial constraints on emissivity while also confirming redshifts through CO lines and assessing their contribution to continuum photometry (e.g. see Smail et al. 2011).

With this superb data, infrared SED fits can be significantly refined. Better photometric constraints mean that more free parameters can be reintroduced into SED fitting, providing a more concrete physical context. What does the value of β imply for the distribution of cold dust? What does the value of α imply for the radial dust distribution? Is there a wavelength regime where the assumption of a powerlaw distribution of warm dust temperatures does not hold, and is that in turn related to the dust distribution or presence/lack of a luminous AGN? Are any galaxies better fit with two independent greybodies rather than one, and does this indicate two distinct dust reservoirs not yet mixed?

Furthermore, interferometers like ALMA will make it routinely possible to resolve dust emission on kpc scales within distant galaxies (as the Submillimeter Array, SMA, has done for some local ULIRGs; Wilson et al. 2008). Spatial mapping of the dust distribution in multiple infrared channels can then be used to assess the mid-IR powerlaw inferred dust distribution. Combined with resolved molecular gas maps obtained through CO emission, routine tests of the Schmidt-Kennicutt relation (Schmidt 1959; Kennicutt 1998) can be performed on a variety of galaxy types at different stages of their star formation histories.

A further refinement which can be made to SED fitting described in this paper is the introduction of PAH emission and Si absorption modeling on top of the suggested dust continuum. Given the wide variety of mid-infrared properties for infrared starbursts, this modeling is best fit independently from the mid-infrared powerlaw dust continuum. This decoupling of the two will be possible with deep near- and mid-IR data from the James Webb Space Telescope (JWST).

5 DISCUSSION & CONCLUSIONS

The characterization of infrared-bright galaxies has become increasingly important in recent years with the introduction of new mid- to far-infrared observing facilities, including *Herschel Space Observatory* and the Atacama Large Mil-

limeter Array (ALMA). Infrared SED fitting techniques vary widely in the literature, from simple greybody fits to detailed dust emission modeling templates.

Section 2.1 has presented an SED fitting technique which can be used to fit a wide range of IR data, from sources which have only 3 IR photometric points to sources with >10 photometric points. These SED fits do not account for PAH emission in the mid-infrared, although they produce accurate estimates to a source's integrated IR luminosity, dust temperature and dust mass. The fitting technique is based on a single dust temperature greybody fit linked to a mid-infrared powerlaw, fit simultaneously to data across $\sim 5\text{-}2000\mu\text{m}$. Without inclusion of the mid-infrared powerlaw, dust temperatures are overestimated and the short-wavelength data ($<50\mu\text{m}$) fit is likely very poor. From the measurement of the mean mid-infrared powerlaw slope α , the dust radial density profile in most local (U)LIRGs is fairly shallow, $\approx r^{-1/2}$. IDL code for the fitting procedure has been made publicly available.

This SED fitting procedure is contrasted with fits to infrared template libraries generated through dust-grain modeling, including those of Chary & Elbaz (2001), Dale & Helou (2002) and Siebenmorgen & Krügel (2007). SED fit quality is categorized by goodness of fit to the GOALS local LIRG and ULIRG sample photometry reported in U et al. (2012). Since the GOALS sources are the most extensively surveyed infrared galaxies to date, they provide a good testbed for SED fitting reliability. The SED templates and original formulation of luminosity for the RBGS sample do not fit the data as well as the fitting method described in section 2.1, leading to overestimated IR luminosities by 10%. Similarly, dust temperatures estimated for the original RBGS sample (Sanders et al. 2003) were overestimated by $\sim 10\text{K}$, due to the different fitting method used (single greybody versus single greybody plus mid-IR powerlaw). Dust temperatures cannot be well constrained with SED templates because they are quantized and only peak at certain wavelengths corresponding to fixed dust temperatures. Clarification is offered on the calculation of dust mass, its dependence on dust temperature, and the lack of correlation between dust mass and IR luminosity.

This comparative study should be useful to highlight some of the current problems facing FIR SED fitting techniques, and the details often overlooked in ambitious analyses of infrared-galaxy population trends for galaxies both near and far.

ACKNOWLEDGEMENTS

The author is grateful for support from a Hubble Fellowship provided by Space Telescope Science Institute, grant HST-HF-51268.01-A. This work would not have been possible without the many constructive conversations about SED fitting and dust properties with Nick Scoville, Vivian U, Alex Conley, Ed Chapin, and Jonathan Williams. Special thanks to Ezequiel Treister, Vivian U and Dave Sanders for inspiring this comparative study, and many thanks to the anonymous reviewer who offered very constructive comments improving the paper.

REFERENCES

- Abel T., Wandelt B. D., 2002, MNRAS, 330, L53
 Armus L. et al., 2009, PASP, 121, 559
 Blain A. W., Barnard V. E., Chapman S. C., 2003, MNRAS, 338, 733
 Blain A. W., Smail I., Ivison R. J., Kneib J., Frayer D. T., 2002, Phys. Rep., 369, 111
 Bolzonella M., Miralles J., Pelló R., 2000, A&A, 363, 476
 Bradford C. M. et al., 2009, ApJ, 705, 112
 Brandl B. R. et al., 2006, ApJ, 653, 1129
 Bruzual G., Charlot S., 2003, MNRAS, 344, 1000
 Calzetti D., 2001, PASP, 113, 1449
 Calzetti D., Kinney A. L., Storchi-Bergmann T., 1994, ApJ, 429, 582
 Casey C. M. et al., 2009, MNRAS, 399, 121
 Casey C. M. et al., 2011, MNRAS, 415, 2723
 Chabrier G., 2003, PASP, 115, 763
 Chapin E. L. et al., 2011, MNRAS, 411, 505
 Chapin E. L., Hughes D. H., Aretxaga I., 2009, MNRAS, 393, 653
 Chapman S. C. et al., 2003, ApJ, 585, 57
 Chapman S. C., Blain A. W., Smail I., Ivison R. J., 2005, ApJ, 622, 772
 Chapman S. C., Smail I., Blain A. W., Ivison R. J., 2004, ApJ, 614, 671
 Chary R., Elbaz D., 2001, ApJ, 556, 562
 Conley A., et al., 2011, ApJL, 732, L35
 Dale D. A., Helou G., 2002, ApJ, 576, 159
 Dale D. A., Helou G., Contursi A., Silbermann N. A., Khatkar S., 2001, ApJ, 549, 215
 Draine B. T., 2006, ApJ, 636, 1114
 Draine B. T. et al., 2007, ApJ, 663, 866
 Draine B. T., Li A., 2007, ApJ, 657, 810
 Dunne L., Eales S., Ivison R., Morgan H., Edmunds M., 2003, Nature, 424, 285
 Dunne L., Eales S. A., 2001, MNRAS, 327, 697
 Hayward C. C., Jonsson P., Kereš D., Magnelli B., Hernquist L., Cox T. J., 2012, ArXiv e-prints
 Hildebrand R. H., 1983, QJRAS, 24, 267
 Hinshaw G. et al., 2009, ApJS, 180, 225
 Kennicutt, Jr. R. C., 1998, ApJ, 498, 541
 Kovács A. et al., 2010, ApJ, 717, 29
 Kroupa P., 2001, MNRAS, 322, 231
 Le Floch E. et al., 2005, ApJ, 632, 169
 Leitherer C., Heckman T. M., 1995, ApJS, 96, 9
 Maraston C., 2005, MNRAS, 362, 799
 Marsden G. et al., 2011, MNRAS, 417, 1192
 Menéndez-Delmestre K. et al., 2009, ApJ, 699, 667
 Neufeld D. A., 1991, ApJL, 370, L85
 Pope A. et al., 2008, ApJ, 675, 1171
 Pope A. et al., 2006, MNRAS, 370, 1185
 Rieke G. H., Alonso-Herrero A., Weiner B. J., Pérez-González P. G., Blaylock M., Donley J. L., Marcillac D., 2009, ApJ, 692, 556
 Roseboom I. G. et al., 2012, MNRAS, 419, 2758
 Salpeter E. E., 1955, ApJ, 121, 161
 Sanders D. B., Mazzarella J. M., Kim D.-C., Surace J. A., Soifer B. T., 2003, AJ, 126, 1607
 Sanders D. B., Mirabel I. F., 1996, ARA&A, 34, 749
 Schmidt M., 1959, ApJ, 129, 243
 Scoville N. Z., Kwan J., 1976, ApJ, 206, 718

- Siebenmorgen R., Krügel E., 2007, *A&A*, 461, 445
Silva L., Granato G. L., Bressan A., Danese L., 1998, *ApJ*, 509, 103
Smail I., Swinbank A. M., Ivison R. J., Ibar E., 2011, *MNRAS*, 414, L95
Swinbank A. M. et al., 2010, *Nature*, 464, 733
U V., et al., 2012, *ApJS*, XXX, XXX
Weingartner J. C., Draine B. T., 2001, *ApJ*, 548, 296
Wilson C. D. et al., 2008, *ApJS*, 178, 189
Younger J. D. et al., 2009, *MNRAS*, 394, 1685